



Brian Fischer

Basic Rules for Indoor Anechoic Chamber Design

Vince Rodriguez

Every year, many requests for proposals for an anechoic chamber are generated by companies and institutions that perform antenna measurements. The task of adequately specifying performance for an indoor anechoic chamber without driving unnecessary costs or specifying contradictory requirements requires insight that is not always available to the author of the specification. Although there are some articles and books that address anechoic chamber design [1]–[3], a concise compendium of reference information and rules of thumb on the subject of specifying ranges would be useful.

This article intends to be a helpful tool in that regard. It starts by recommending the proper type of range for different antenna types and frequencies of operation. Rules of thumb are provided to select the best approach for the required test or antenna type. Information is provided on the derivations needed for other ranges, such as compact ranges and near-field test facilities. Simple approximations are used for absorber performance to generate a series of charts that can be used as a guide to specify anechoic chamber performance and size. Company and

EDITOR'S NOTE

Most readers of the “Measurements Corner” column will be very familiar with anechoic chambers as users, but many may not understand the numerous design trades that go into their construction. This issue’s column captures key requirements and trades that one must consider when preparing to procure a new chamber.

institution facilities can then define the appropriate square footage necessary to house the required antenna range. This article intends to avoid some of the common contradictory requirements. Some of these contradictory requirements are not enough real estate to accommodate a chamber operating at low frequencies or levels that are not possible given available absorber technology.

THE ANECHOIC CHAMBER

The ability to measure an antenna is an important design requirement. It is imperative to know whether the energy is radiating properly and in the desired direction per the design specifications. It is also important to know how much energy is traveling in undesired directions. To measure antennas (like many other devices that are being measured), there is the desire to have the antenna unaffected by its surrounding environment. This is where the anechoic chamber becomes a viable solution. The anechoic

chamber provides an environment that is free of echoing or other radiated signals and reduces the effects of these undesirable signals during the testing of a given antenna. This article covers applications where an antenna is radiating or receiving a given signal while we want to know its performance as a function of direction. Excluded from this discussion are anechoic chambers for measuring radar cross section. The general range geometry is shown in Figure 1.

RANGE TYPE SELECTION

There are several methods of measuring the radiation patterns of antennas indoors: far-field illumination, near-field measurements, and compact range (CR). Like many other solutions, there are pros and cons for each of these. There is not a single solution that is ideal for all types of antennas and situations. The type of range that is most suitable for a given type of antenna is determined based on two parameters: the frequency and the electrical size of the antenna under test (AUT).

The far-field condition given by the following equation drives the selection:

$$r \geq \frac{2 \cdot D^2}{\lambda}. \quad (1)$$

The previously mentioned parameters are embedded into the far-field equation. D is the largest physical dimension of the antenna. The wavelength is shown as λ , which is related to the frequency of operation on the antenna. As noted in [4], for smaller antennas, the far-field range length, r , can be approximated by

$$r \approx 10\lambda. \quad (2)$$

Equation (2) can be used when the antenna is under one wavelength in electrical size. Going back to (1), the far-field distance can be plotted as a function of the electrical size of the antenna. This is shown in Figure 2. As a rule of thumb for indoor ranges, we can state that far-field illumination techniques are better suited for antenna sizes under ten wavelengths. This rule is related to the electrical antenna size. The frequency of operation adds another factor that will influence the type of range. Figure 2 shows that an antenna with a size of 10λ will have a far-field distance of 200λ , so the test distance is 20 times the size of the antenna; at some microwave frequencies, this may be a test distance of 200 in (5 m), so an indoor range may be easy to implement. However, a 20λ antenna will have a test distance that is 800λ .

For example, consider an 18-in dish that is used by a popular satellite television (TV) service. This satellite service operates at 18.55 GHz. The dish antenna is 28.29λ in size. The far field is at approximately 1600λ or 25.86 m (84.84 ft). Clearly, for such an electrically large antenna, a far-field illumination approach indoors is not economically feasible. For this antenna, a CR or a near-field approach is more suitable. Conversely, a ten-wavelength antenna at 300 MHz, which is 10 m in size, would be extremely difficult to manipulate, and the test distance will be 200 m. For this case, the best solution would be an outdoor range. As will also be discussed in the next section, current absorber technology does

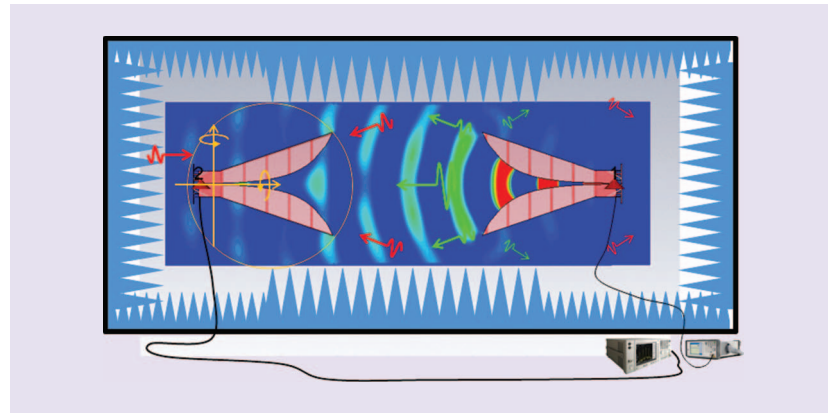


FIGURE 1. The general geometry of an indoor range. Two antennas are located in the range: one for transmitting and one for receiving.

not support some indoor measurements at those low frequencies. Thus, there is a lower frequency boundary for indoor ranges. In general, for frequencies below 100 MHz, an outdoor range is a better approach. Indoor ranges can be built, but the antenna size should be kept lower than 2λ , which limits the far-field distance to 8λ (24 m). This distance is close to the 10λ given by (2); Table 1 provides an approximate guide for the different antenna sizes and frequencies of operation.

The values in Table 1 are general guidelines. Spherical near-field (SNF) ranges can test antennas as small as $\lambda/2$, but for such a small antenna, the better approach may be to use a far-field illumination range. When

selecting the range, it is important to think of the typical electrical size of the AUT. When creating an anechoic chamber, the goal is to obtain a volume in the chamber where any reflected energy from the walls of the range (ceiling and floor) will be much lower than any of the features of interest on the radiation pattern. This volume is what it is known as the *quiet zone* (QZ). Figure 1 shows that as one antenna transmits, it illuminates the receive antenna and all the walls and surfaces of the range. As described in [1] and [3], the energy incident on these surfaces will be reflected toward the QZ. The level of reflected energy must be a given number of decibels below the

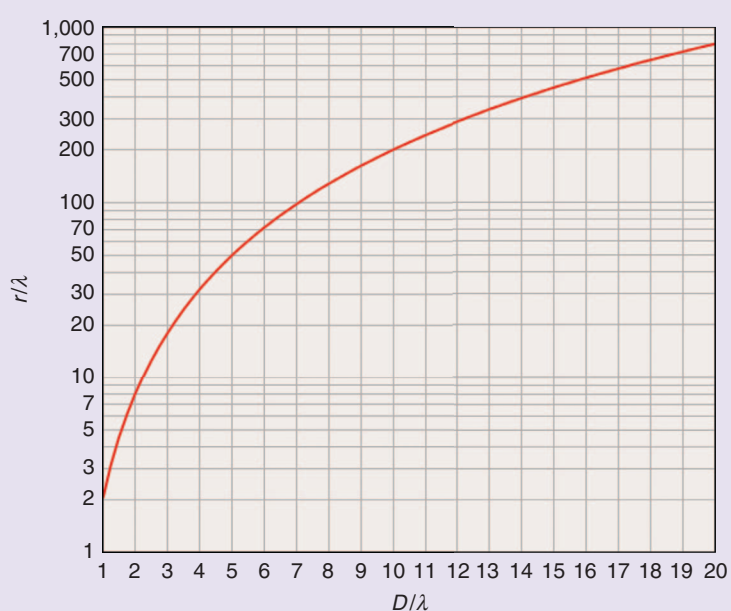


FIGURE 2. The far-field distance plotted in relation to the wavelength.

TABLE 1. FREQUENCY RANGES AND ANTENNA SIZES FOR THE DIFFERENT INDOOR ANTENNA MEASUREMENT APPROACHES.

| Indoor Ranges | | Antenna Size in Wavelengths | | |
|---------------|------------------------|-----------------------------|---------------|---------------|
| Frequency | Far-Field Illumination | Near-Field Measurements | Compact Range | |
| 100 MHz | $< 2\lambda$ | $> 2\lambda$ | | Not ideal |
| 500 MHz | $< 2\lambda$ | $> 2\lambda$ | | Not ideal |
| 1 GHz | $< 5\lambda$ | $> 5\lambda$ | | $> 5\lambda$ |
| 2 GHz | $< 10\lambda$ | $> 10\lambda$ | | $> 10\lambda$ |
| ≥ 4 GHz | $< 10\lambda$ | $> 10\lambda$ | | $> 10\lambda$ |

direct path between the transmitting and the receiving antennas.

Consider the setup in Figure 3. As the antenna being measured is rotated, its main beam will illuminate different surfaces of the chamber. The range antenna will measure the level of field radiated by the AUT along the direct path between the two antennas. However, the range antenna will also receive the reflected energy from the walls, ceiling, and floor. If the reflected energy level is higher than the energy radiated along the direct path between the two antennas, then the radiation pattern in that direction cannot be measured accurately. In Figure 3, the measuring antenna (also known as the *range antenna* or *source*

antenna) is pointing at a null, but it is also receiving the reflected signal from the wall that is illuminated by the main beam of the AUT. The range antenna is receiving the reflected signal in a direction of 30°. In that 30° direction, the gain of the range is lower than in the direct path (boresight) to the AUT. Let us assume that the antenna gain in the 30° direction is 10 dB lower than the boresight. The reflected energy is a number of decibels lower; let us assume 20 dB. The signal received by the antenna on that direction will be -30 dB compared to the energy received when the main beam of the AUT was pointing to the range antenna. If the null is lower than -30 dB, then the range antenna

will not measure that level. The error in the antenna pattern from the reflected energy is discussed in [5] and [6].

RADIO-FREQUENCY ABSORBER

A key design item for an anechoic chamber is the radio-frequency (RF) absorber. The absorber treatment must be such that the reflected energy has a small or negligible effect on the measured data. A typical RF absorber is a lossy material shaped to allow for the incoming electromagnetic wave to penetrate the lossy material with minimal reflections. Once the electromagnetic energy travels inside the material, the energy transforms into thermal energy and dissipates into the surrounding air [7]. The electrical thickness of the material determines how much energy is absorbed. The reflection level at a normal incidence can be approximated by

$$R_o(t) = -13.374 * \ln(t) - 26.515, \quad (3)$$

where t is the thickness in wavelengths. The equation is valid for $0.25 \leq t \leq 20$. This approximation can be used to get a conservative approximate value of the reflectivity of the absorber of a given thickness. Most manufacturers provide the information in their data sheets.

Figure 1 shows that some of the absorber in the range is not located in a position where the incident wave is in the normal incident direction but, rather, in an oblique incidence. For an oblique incidence, the main reflectivity of the absorber is in the bistatic direction. Backscattering occurs when the distance between the tips of the pyramids is $\geq \lambda$ as demonstrated in [8]. In [1], Hemming provides plots that show the estimated bistatic reflectivity of the absorber at the oblique incidence. In this article, we introduce a series of polynomial approximations that, together with (3), provide a general description of the performance of a pyramidal absorber with different thickness and at different angles of incidence. These are approximations, and they err on the conservative side. That leaves a margin of error to account for things like lights, doors, positioning equipment,

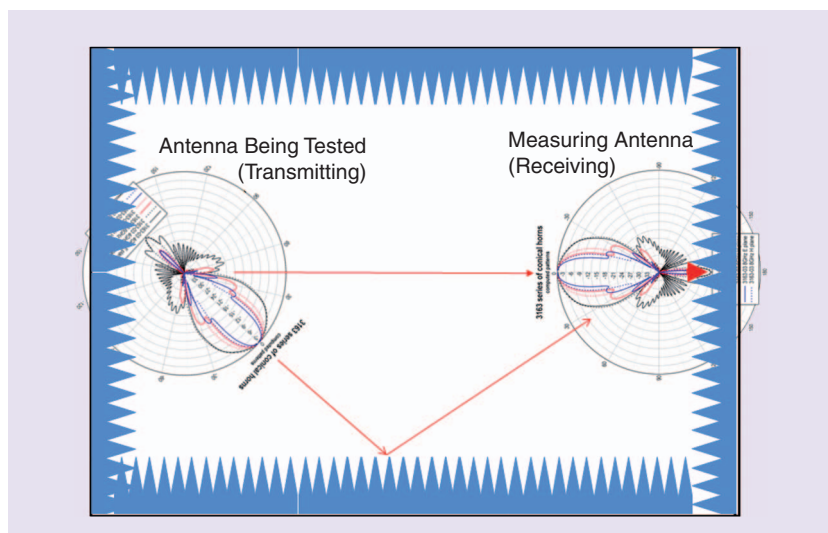


FIGURE 3. An indoor range showing one of the reflected paths and the direct path between the AUT and the source antenna.

and edge diffractions from treatment discontinuities.

The absorber performance in decibels is given by the following polynomial:

$$R_\theta(t, \theta) = R_0(t) + A_1(t) \cdot \theta + A_2(t) \cdot \theta^2 + A_3(t) \cdot \theta^3 + A_4(t) \cdot \theta^4 + A_5(t) \cdot \theta^5. \quad (4)$$

The coefficients in (4) are functions of the thickness. When the thickness of the absorber is such that $0.25\lambda \leq t \leq 2\lambda$, then the coefficients of (4) are given by the following polynomials:

$$A_1(t) = 1.5252 - 4.8243t + 6.9479t^2 - 3.8332t^3 + 0.7333t^4, \quad (4a)$$

$$A_2(t) = -0.0754 + 0.24782t - 0.3984t^2 + 0.2285 - 0.0442t^4, \quad (4b)$$

$$A_3(t) = 0.0016 - 0.00502t + 0.00938t^2 - 0.00577t^3 + 0.001155t^4, \quad (4c)$$

$$A_4(t) = -1.58 \cdot 10^{-5} + 4.91 \cdot 10^{-5}t - 1.015 \cdot 10^{-4}t^2 + 6.58 \cdot 10^{-5}t^3 - 1.35 \cdot 10^{-5}t^4, \quad (4d)$$

$$A_5(t) = 5.84 \cdot 10^{-8} - 1.78 \cdot 10^{-7}t + 4.02 \cdot 10^{-7}t^2 - 2.71 \cdot 10^{-7}t^3 + 5.7 \cdot 10^{-8}t^4. \quad (4e)$$

When the thickness of the treatment is such that $2\lambda \leq t \leq 20\lambda$, then the coefficients are given by the following set of polynomials:

$$A_1(t) = 0.1751 + 0.149t - 0.0119t^2 + 0.00028t^3, \quad (4f)$$

$$A_2(t) = -0.0105 - 0.00824t + 0.0007t^2 - 1.61 \cdot 10^{-5}t^3, \quad (4g)$$

$$A_3(t) = 0.00029 + 0.000123t - 1.13 \cdot 10^{-5}t^2 + 2.57 \cdot 10^{-7}t^3, \quad (4h)$$

$$A_4(t) = -1.69 \cdot 10^{-6} - 4.77 \cdot 10^{-7}t + 5.08 \cdot 10^{-8}t^2 - 1.14 \cdot 10^{-9}t^3, \quad (4i)$$

$$A_5(t) = 0. \quad (4j)$$

The domain of (4) is limited by those angles of incidence where $0^\circ \leq \theta \leq 85^\circ$ and where $\theta = 0^\circ$ is a normal incidence. Additionally, the domain is limited by the domain of the coefficient

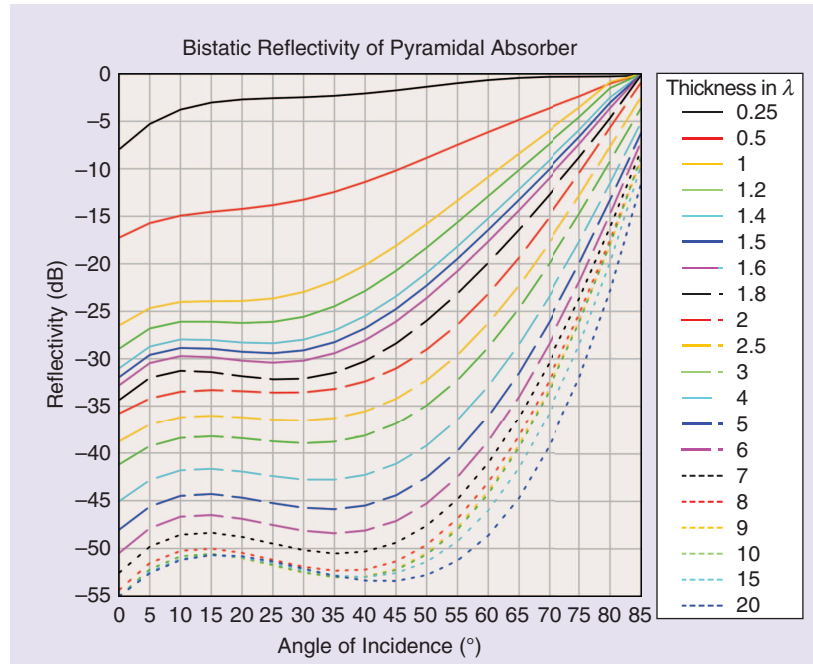


FIGURE 4. The estimated reflectivity of an RF absorber as a function of an angle of incidence.

polynomials. Hence, (4) is valid when $0.25\lambda \leq t \leq 20\lambda$, as stated previously. The range of (4) should also be limited to $-55 \geq R(\text{dB}) \geq 0$. For an absorber of thickness larger than 20λ , the reflectivity can be approximated using the results for a 20λ -thick absorber. Figure 4 shows the bistatic performance as a function of the angle of incidence for a series of different electrical thicknesses of the absorber. Figure 5 shows a comparison of computed results using the method in [9], given manufacturer specifications and the results from (4) for a material of thickness equal to λ and 2λ .

If we compare the results of the polynomials presented in this article to those from numerical computations, we can see that the polynomials provide a conservative number for the reflectivity that may be higher by about 10 dB. The manufacturer specifications were only provided from 45° to 80° and for a normal incidence. Computed results were obtained only at a few angles. For the 1λ -thick absorber, the different methods follow similar trends, with the polynomials providing the most conservative number. There is a large difference at 35° between the computed

and the polynomial results. However, that null in the reflectivity may shift depending on the material in which the absorber is mounted, as shown in [10]. In general, the polynomials are a safe approximation for the performance of RF materials at different angles of incidence.

The largest typical absorber size currently available is 72 in (1.82 m). As was mentioned previously, this size provides a frequency limit for the use of indoor ranges. At 100 MHz, the thickness of this absorber is 1.64λ . Its normal incidence performance is about -33 dB. In an indoor range lined with this material pattern, features -20 dB from the peak will be difficult to measure accurately. There are hybrid absorbers merging ferrite tiles and lossy substrate pyramids or wedges that operate down to 30 MHz or even 20 MHz. These types are more suitable for electromagnetic compatibility applications as their normal-incidence absorption is typically limited to 25 to 35 dB.

RANGE SIZE

The discussion regarding sizing the range begins with rectangular far-field ranges, which have a test distance

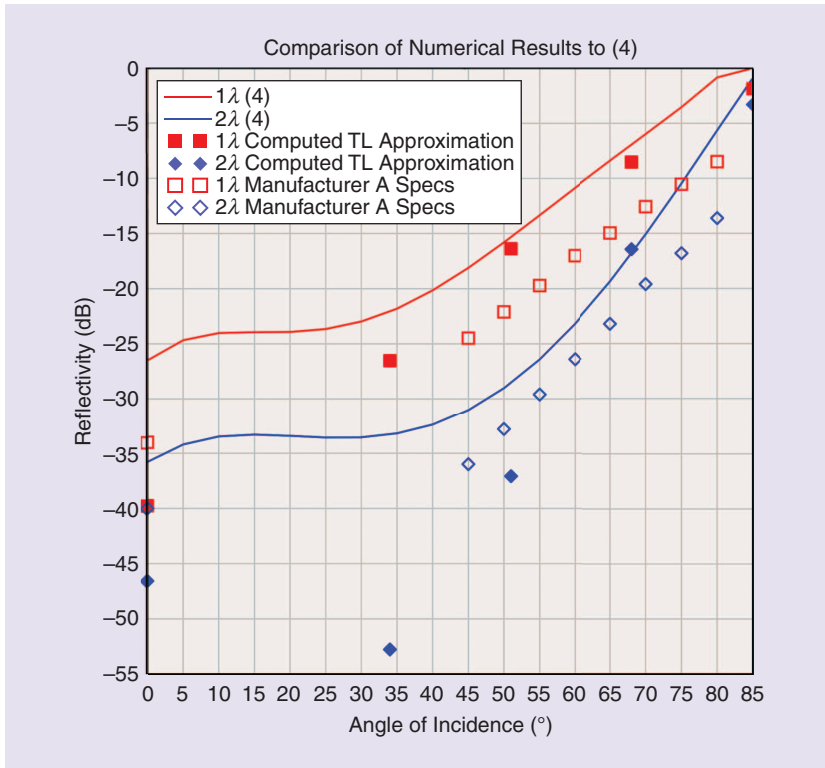


FIGURE 5. A comparison of bistatic reflectivity from a computational approach, manufacturer's specifications, and (4).

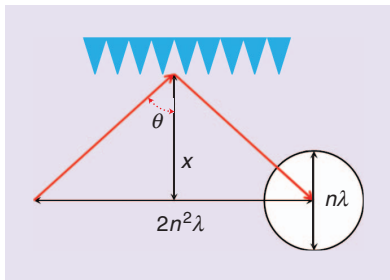


FIGURE 6. The geometry of a far-field range.

determined by (1). Following the discussion on far-field ranges, CRs and near-field ranges will be discussed.

FAR-FIELD CHAMBERS

It is common to find sources stating the rules of thumb for sizing a rectangular anechoic chamber for far-field illumination; these can be found in [1]. The general rule is that the width and height of an anechoic chamber should be three times the diameter of the minimum sphere that contains the largest antenna being tested. It is important to check that a minimum spacing of 2λ between the AUT and the tips of the absorber

is maintained. This minimum spacing avoids loading of the AUT. The far-field distance is given by

$$\frac{r}{\lambda} = 2n^2, \quad (5)$$

where n is the number of wavelengths in the size of the AUT. The QZ must be large enough to encompass the AUT. Hence, the QZ is $n\lambda$. Figure 6 shows a typical rectangular range geometry.

From the geometry in Figure 6, we can derive an equation for the distance x . The distance x is the distance from the range centerline to the absorber tips.

$$\frac{x}{\lambda} = n^2 \cdot \cot \theta. \quad (6)$$

Equation (6) gives the distance in terms of wavelengths. If we look at Figure 3, the value of θ can be chosen to give a desired reflectivity. The curves in Figure 4 will also provide a value for the thickness of the absorber. Hence, if the AUT has features that need to be measured in the -25 dB level, then the bistatic reflectivity of the absorber must exceed that level. An absorber 2λ in thickness will exceed

-25 dB up to angles of 50° . Hence, the width of the chamber is

$$2x = (2n^2(0.84) + 4)\lambda, \quad (7)$$

where the added four accounts for the 2λ thickness of the absorber. If a different thickness of absorber is used, (7) will change. In general, the chamber width can be written as

$$W = (2n^2 \cot(\theta) + 2t)\lambda. \quad (8)$$

Parameters θ and t must be chosen to obtain the required reflectivity. It is important to check that the minimum 2λ spacing from the QZ to the absorber is kept. The length of the rectangular far-field chamber is mainly given by the far-field distance and the QZ size plus the absorber thickness and at least a spacing of 2λ between the QZ and the absorber. Added space should be included for the range antenna and for the absorber behind it.

The total chamber or range length (L) is given by

$$L = (2n^2 + n + 2 + t + K)\lambda, \quad (9)$$

where K is a factor large enough to include the source antenna, the spacing to the absorber, and the absorber behind the source. It should be noted that these equations provide a minimum requirement. Work must be performed inside the chamber, mounting and connecting the antenna, switching range antennas, etc. The space should be checked to allow for people to perform these tasks inside the anechoic range.

Let us enter some values into the prior equations to observe the expected chamber sizes. It will be assumed that the source antenna is directive and that it has a sufficient front-to-back ratio. The absorber behind the source antenna will be one wavelength in thickness, and the factor K will be set to four. In Figure 7, the width and length of a series of rectangular chambers have been plotted versus the lowest frequency of operation. In addition, the electrical size of the AUT at the lowest frequency is indicated by the value of n for each plotted chamber size.

From Figure 7, there are some conclusions that can be drawn. The first is

if a chamber is designed for an antenna of given $n\lambda$ at the lowest frequency, that same chamber is large enough for testing antennas of the same electrical size at higher frequencies. But similarly, we see that, as we go lower in frequency, the chamber size must increase for a given electrical size. At 500 MHz, a chamber for a 2λ -sized antenna is planned to be about $10 \text{ m} \times 5 \text{ m}$. If the antenna size was increased to 4λ , the chamber would need to be $18 \text{ m} \times 10 \text{ m}$. Tapered anechoic chambers should be used at these lower frequencies as reported in [1] and [11]–[13]. The geometry of the taper chamber uses the specular reflection off the side walls for the AUT illumination rather than reducing its level as it is done in the rectangular chamber. This leads to a physically smaller chamber.

The height of the chamber should be the same as the width of the chamber. By doing this, the reflections from the ceiling and floor will be similar in level. This is important since the reflected energy from the ceiling and floor will be similar, and the effects of the range on polarization depended parameters such as cross polarization and axial ratio will be minimized. Equations (8) and (9) provide a good idea of the space requirements for an indoor range. In most cases, a chamber size can be adjusted. For example, the absorber on the ceiling and floor can be increased in thickness to maintain the reflectivity at more oblique angles of incidence (larger θ). Chebyshev arrangements [14] of the absorber layout can also be used to improve reflectivity. Figure 3 also gives us another clue to improve the reflectivity. The reflected ray arrives at the range antenna at an angle at which the gain of the antenna is lower than in the boresight direction. Using higher directivity antennas as sources reduces the amount of energy received from the side walls, ceiling, and floor. Hence, a shorter absorber may be used, thus reducing the chamber size.

TAPER ANECHOIC CHAMBERS

Taper chambers have been described previously in the literature [3]. In these chambers, the specular bistatic reflectivity is not minimized as it is done on rectangular chambers, but it is used to

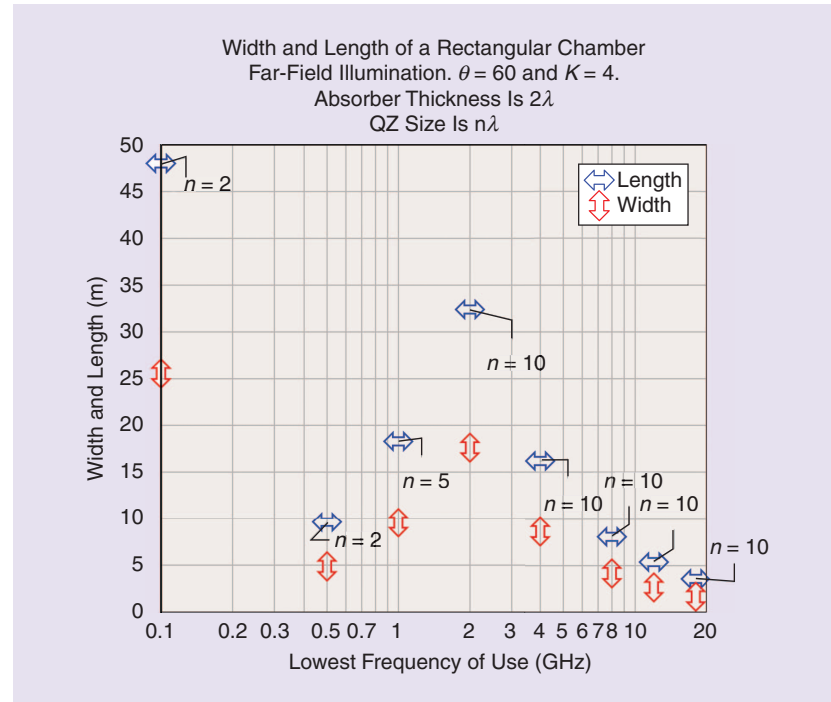


FIGURE 7. The rectangular far-field chambers for different lowest frequencies of operation and different largest-size antennas at their lowest frequencies.

illuminate the QZ. In general, the rules for sizing a tapered chamber are empirical, and they have been reported in [1]. The approach this article follows is to set the back wall absorber to a thickness that provides a reflectivity that slightly exceeds the requirements for the QZ at the lowest frequency. Hence, if the requirements call for a reflectivity of -40 dB at the lowest frequency, Figure 4 shows that a 4λ absorber will provide and exceed that requirement. The height and width of the rectangular section of the tapered chamber are given by

$$W = H = QZ + 4\lambda + t\lambda, \quad (10)$$

where $t\lambda$ is the thickness of the back wall absorber; that is, the absorber on the side walls, ceiling, and floor are half the thickness of the back wall absorber. The 4λ in (10) provides the 2λ spacing between the QZ and the tips of the absorber. And QZ is the diameter of the QZ. The length of this rectangular section of a taper chamber is given also by (10). This makes the rectangular section a cube, which is commonly seen and as is also shown

in [1]. This is usually an acceptable approach since these tapered chambers operate at low frequencies, and the wavelength spacing between the QZ and the tips of the absorber is large enough for personnel access to the QZ and for the AUT positioner to operate without hitting the absorber. In some cases, the spacing between the QZ and tips of the absorbers can be as small as a single wavelength (at the lowest frequency).

The taper section has a simple equation to evaluate its length. The equation is based on the 30° angle for the taper given in [1]. This angle was selected empirically. We prefer to use 28° as the angle; hence, the maximum length for the taper section is given by

$$L_{\text{taper}} = 4 \frac{W}{2}, \quad (11)$$

where W is the width of the rectangular section. The overall length required for the taper chamber will be L_{taper} added to W since the length of the rectangular chamber is the same as the width (assuming a cubical rectangular section). Figure 8 shows a typical taper chamber geometry.

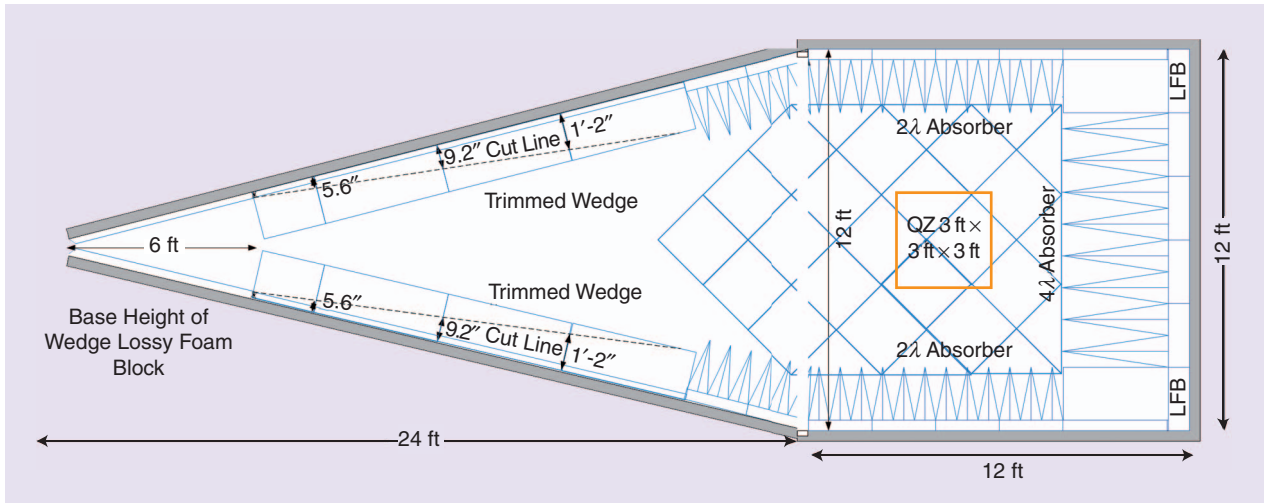


FIGURE 8. A typical tapered anechoic range.

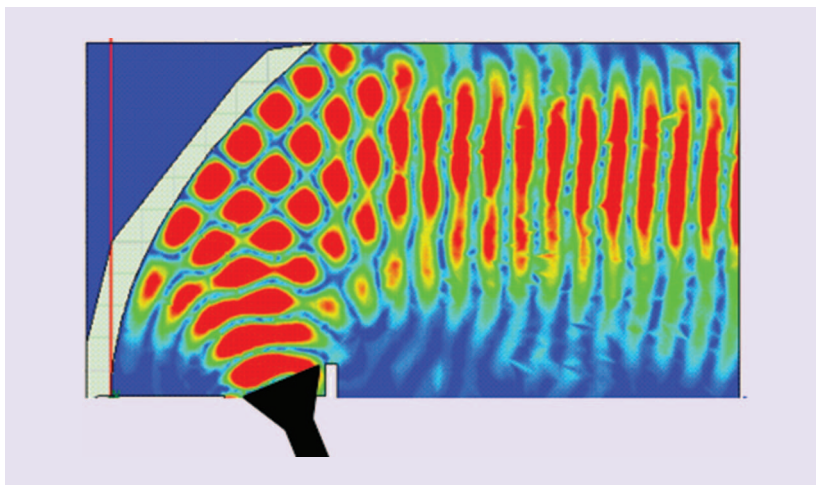


FIGURE 9. The simulated results of a parabolic reflector. Note the plane wave behavior on the right-hand side of the illustration.

TABLE 2. SIZES AND FREQUENCY RANGES OF COMMERCIALLY AVAILABLE CR REFLECTORS.

| QZ Size (Length and Diameter) | Overall Reflector Size (Including Serrations) | Length of Serrations | Frequency of Operation | Focal Length f |
|----------------------------------|--|----------------------|------------------------|------------------|
| 61 cm | 216 cm × 188 cm | 38 cm | 4–200 GHz | 182 cm |
| 122 cm | 432 cm × 335 cm | 76 cm | 2–200 GHz | 366 cm |
| 182 cm | 488 cm × 416 cm | 76 cm | 2–200 GHz | 366 cm |
| 244 cm | 864 cm × 670 cm | 152 cm | 1–200 GHz | 732 cm |
| 366 cm | 975 cm × 833 cm | 152 cm | 1–200 GHz | 732 cm |

COMPACT RANGES

Although barely mentioned in [5], the CR has become an important tool in measuring electrically large antennas.

The satellite TV antenna described in the “Rate Type Selection” section is close to 20λ in size and common in satellite communication and radar applications.

There is a need for testing these antennas in a controlled, accurate, and secure location. The CR uses a parabolic reflector to create a plane wave illumination at the location of the AUT. This plane wave simulates the field distribution that the antenna would typically experience in the far field. Figure 9 shows a parabolic reflector illuminated by a source located at the focal point of the parabola. The plane wave behavior can be seen at a short distance from the reflector.

The reflector system is the controlling factor when sizing the range. The reflector must be large enough to provide a plane wave that illuminates the entire antenna being tested. In addition, the reflector should be properly terminated. There are different ways of terminating a reflector. The two most common are serrations and rolled edges [15]. The purpose of the termination is to reduce the effects of the terminated paraboloid on the illumination. In the case of serrated edge reflectors, serrations can be between three and five wavelengths at the lowest frequency of operation. Table 2 provides a typical list of reflectors showing their overall size and their frequency range. It should be noted that as frequency increases, the reflector becomes more efficient. While some reflectors can operate well into the millimeter-wave range, extra care should be taken during manufacturing and surface finishing as surface imperfections will affect the performance.

As previously stated, the reflector size is the determining factor when sizing the width and height of the chamber. The length of the chamber will be affected by the focal length of the reflector. The distance from the vertex of the reflector to the QZ is given by the following rule:

$$r = \frac{5}{3}f_l, \quad (12)$$

where f_l is the focal length of the reflector. Referring to our satellite TV antenna example requiring a far-field distance of 25 m to test, one might expect

long chambers and large distances for CR testing. However, Table 2 coupled with (12) indicates the test distance for a 61 cm QZ is 3 m. This is sufficient to test the satellite TV antenna. As a rule, the length of a CR chamber is given by

$$L = R_{clr} + \frac{5}{3}f_l + \frac{1}{2}QZ + (2 + t)\lambda, \quad (13)$$

where R_{clr} is the reflector clearance. This includes the mechanical structure to support the reflector, which ranges from 60 cm to 2 m depending on the overall

reflector size. In general, the wall behind the reflector has a small absorber, usually $\lambda/2$ in thickness, and it only covers the perimeter of the wall. The parameter t is the thickness of the end wall absorber. For a CR, this is the most critical wall and, therefore, should have the lowest reflectivity. It is recommended that the end wall absorber be no less than three to four for the value of t .

The width of the chamber is calculated using a straightforward equation:

$$W = CR_w + (4 + 2t)\lambda, \quad (14)$$

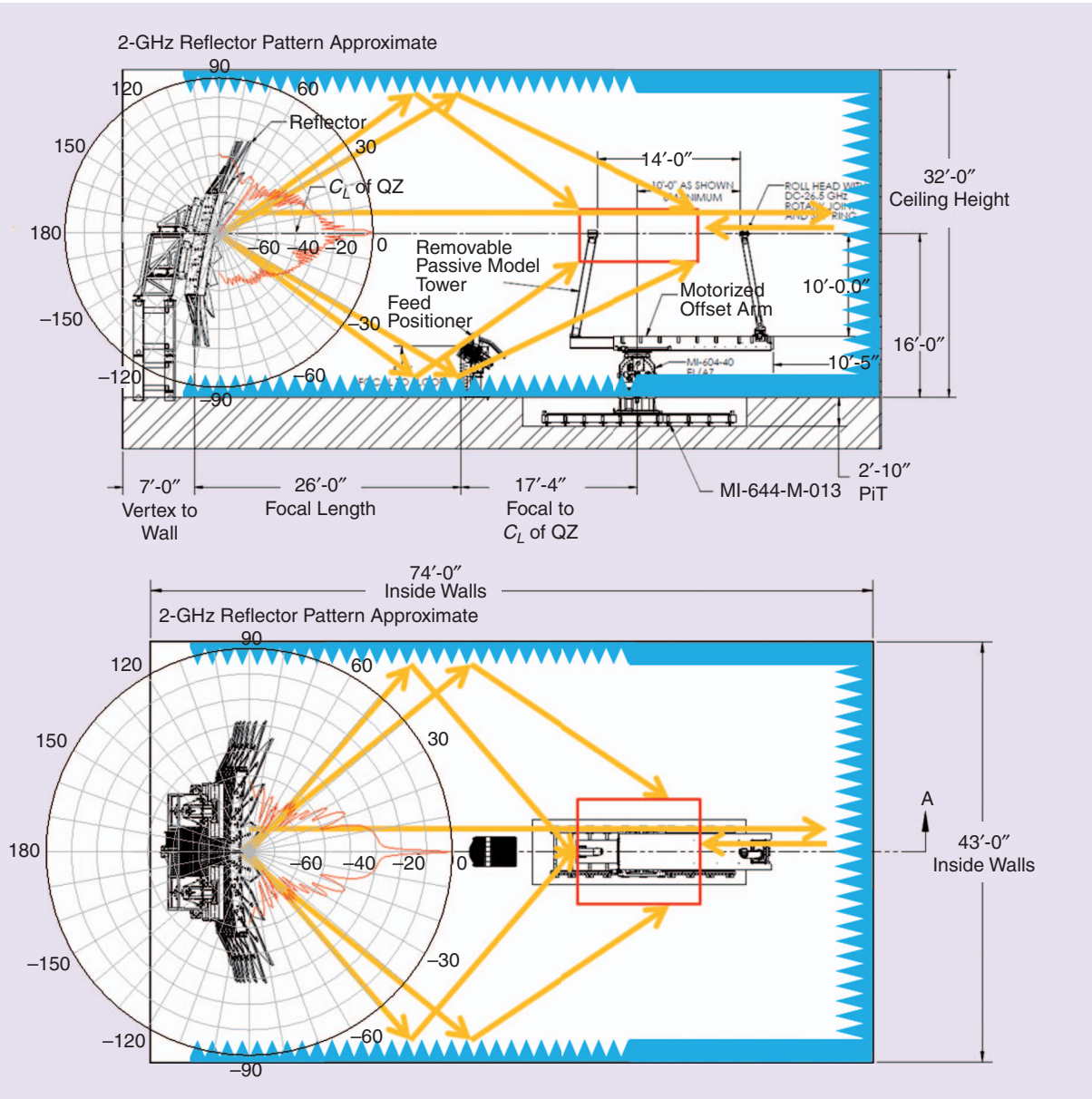


FIGURE 10. A typical CR layout with the reflector pattern superimposed and showing that the energy incident on the side walls, floor, and ceiling is already more than -40 dB down at 2 GHz.

where CR_w is the overall width of the reflector. There is an additional 2λ from the tips of the serrations to the absorber tips on each side of the reflector. Experience has shown that, in some cases, the spacing can be as small as one wavelength on each side. The final item on the width of the range is the thickness of the absorber. While for far-field ranges the absorber on the ceiling, floor, and side walls should be thick enough to provide good bistatic reflectivity at oblique angles, in the CR, the side wall absorber does not need to be as thick. Figure 10 shows a typical CR chamber. The radiation pattern of the CR reflector has been superimposed over the chamber drawing.

The reflector in the picture provides a $3.66 \text{ m} \times 1.82 \text{ m}$ elliptical QZ. The depth of the QZ is 3.66 m. The important aspect of the CR is that it has a very directive pattern, with directivities in excess of 25 dBi. As Figure 10 shows, the energy incident that is on the absorber on the side walls is already -40 dB below the direct path. Looking at Figure 4, a λ thick absorber will provide -10 dB of absorption at over 60° of incidence. Combining the reflectivity with the difference in magnitude between

the direct ray and the reflected ray, we have a reflected energy level in the -50 dB range. This level is an approximation. Clearly, the reflector is being used in the near field while the radiation pattern of the reflector is a far-field concept. However, this is an acceptable approximation as it provides a method for estimating the level of energy that radiates from the reflector in the direction of the walls. Figure 11 shows that the reflector will send some energy toward the side walls. This energy is estimated using the far-field pattern of the reflector.

The height of the chamber has a similar equation for the size

$$H = CR_h + (2 + K + 2t)\lambda, \quad (15)$$

where CR_h is the overall height of the reflector. There are two wavelengths of spacing between the tips of the reflector and the tips of the ceiling absorber. The parameter K provides a factor for the spacing between the floor and the reflector. For the floor absorber, we want a larger separation between the edge of the reflector and the tips of the floor absorber. This reduces the angle of incidence at the specular point between the reflector feed and the reflector

to minimize the impact of the floor reflection on the reflector illumination (see Figure 12). Equation (15) includes K wavelengths of space between the tips of the floor absorber and the serration tips. K shall be large enough to provide enough extra space to provide room for the feed positioner supporting the feed antenna that illuminates the reflector.

As was the case with the side walls, the absorber on the floor and the ceiling can be one wavelength in thickness. Special consideration must be taken for the floor absorber between the feed and the reflector, which may be 2λ in thickness. In general, the absorber electrical thickness (at the lowest frequency) can be $t \leq 1.2$ and $t \geq 0.75$ for the side wall and ceiling treatments of CRs.

NEAR-FIELD RANGES

There are different approaches for performing near-field measurements. The different techniques are related to the type of antenna being measured. In all approaches, the field (amplitude and phase), radiated from the AUT is measured on a surface. After this near-field measurement, the far-field behavior is mathematically obtained. Depending on the surface where the data are measured,

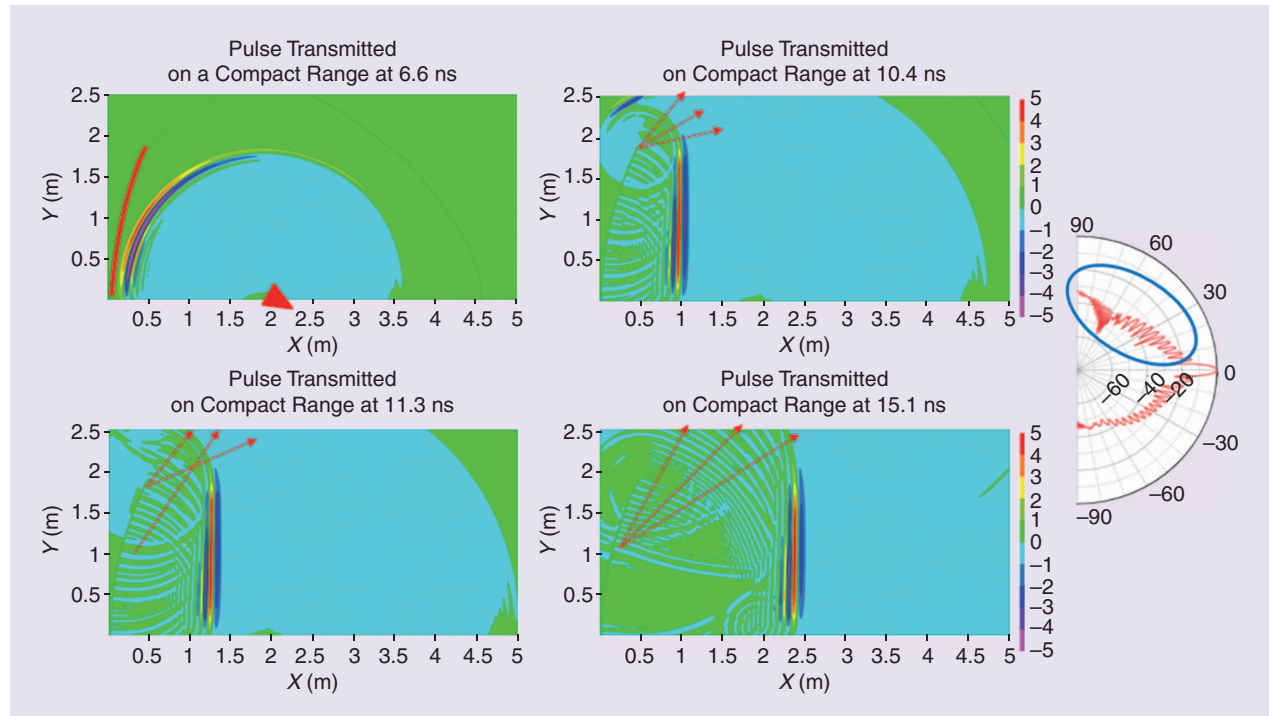


FIGURE 11. Radiation from the reflector compared to the far-field pattern.

three different near-field techniques can be identified: planar (PNF), cylindrical (CNF), and SNF [16], [17]. The most basic near-field measurement approach is planar scanning. In this technique, the field radiated from the antenna is scanned on a single plane. This is a good technique for high-gain antennas as there is a very small amount of energy radiating to the back of the antenna. The second near-field measurement approach is cylindrical scanning. In this technique, the field is measured on the surface of a cylinder excluding the top and bottom surfaces. This technique is ideal for long antennas that are omnidirectional or have a wide beam on one of the principal planes but a narrow beam in the perpendicular plane. The last near-field and more general measurement approach is spherical scanning. In this technique, the field is measured on a sphere that contains the entire antenna being measured. In general, the test distance for planar near-field measurements is between 3λ and 10λ . For SNF, however, the probe can be further away. The SNF is discussed in detail in [18].

The same equations developed for far-field chambers can be used for SNF with the exception of equations for the test distance. In general, the equation is given by

$$L = d_{pp} + (n + 6 + 2t_e)\lambda, \quad (16)$$

where d_{pp} is the depth of the probe (measuring antenna) and its positioner. The variable n is the diameter in wavelengths of the minimum sphere that contains the AUT. The absorber on the two end walls will have a thickness of $t_e\lambda$, where t_e is the thickness, in wavelengths, of the end wall absorber. As customary, 2λ is added between the minimum sphere and the absorber tips, and, finally, we estimate 4λ as the distance between the probe and the sphere containing the antenna. The width of the SNF chamber is given by

$$W = (n + 4 + 2t_s)\lambda, \quad (17)$$

where, in this case, t_s is the thickness in wavelengths of the side wall absorber.

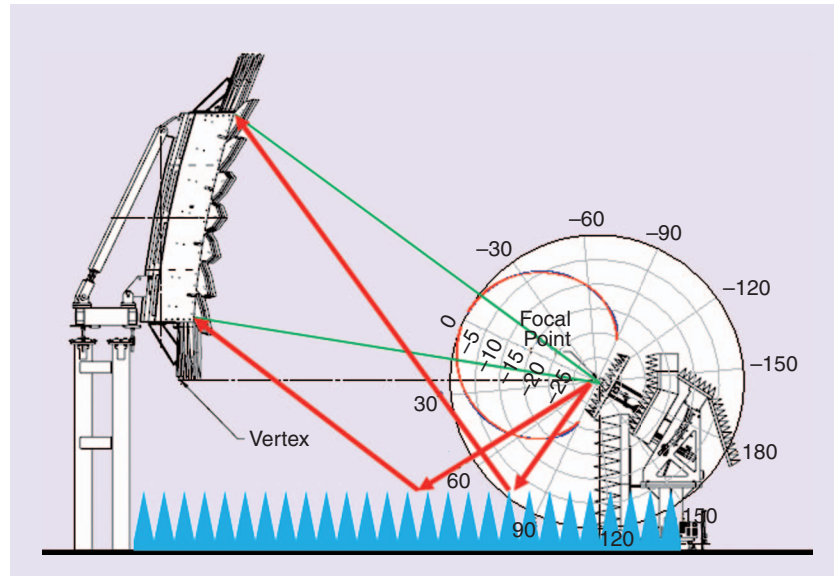


FIGURE 12. The absorber on the floor between the feed positioner and the reflector is critical to reduce the reflected energy from illuminating the reflector.

This is a rough approximation. For both (16) and (17), an additional 1 m minimum should be added to prevent the positioning equipment from hitting the probe as it rotates the antenna being measured. Also, this space should provide room for people to perform work inside the chamber during the set up of the measurement. This is more critical for higher frequencies (above 2 GHz) where the 4λ separation may not be enough for the positioner to clear the probe.

We notice that the angle of incidence on the side absorber is given by

$$\theta = \arctan\left(\frac{4n + 16}{2n + 16}\right). \quad (18)$$

Taking the limit as $n \rightarrow \infty$, it follows that $\theta < 63.4^\circ$. Using Figure 4, we can estimate that $t_s \approx 2t_e$. To do this, we check the reflectivity of the end wall absorber at the normal incidence, and we select the thickness of the absorber that will provide similar reflectivity for the 63.4° incident angle. The ceiling and the floor will have the same absorber as the side walls.

The chamber height can be estimated using

$$H = h_p + (n + 4 + t_s)\lambda. \quad (19)$$

The variable h_p accounts for the height of the positioning equipment. In a typical rollover azimuth positioner that is

used in SNF, h_p should include the height of the floor slide, the azimuth positioner, and the offset slide. The reader should be aware that we have not taken into account the positioning equipment in the far-field chamber equations or the CR equations (except for the feed positioning). The reason being that, in those types of ranges, other dimensions are so dominant (the far-field test distance or the reflector size) that the positioner is not an issue.

PNF systems use a planar scanner to measure highly directive antennas (i.e., gain > 20 dB). The high gain of the AUT benefits in the design of the range, as some regions of the range (those behind the AUT) do not need to be treated with an absorber. The test distance, as stated above, is between three and ten wavelengths. The dominant factor for sizing a PNF range is the scanner. The scan size is given by

$$L_x = (n + 2k \tan(\theta_s))\lambda, \quad (20)$$

where θ_s is the maximum angle for an accurate far field, and $n\lambda$ is the electrical size of the antenna being tested (see Figure 13). The variable k is the test distance in wavelengths, hence, $3 < k < 10$. The physical scanner will usually be slightly larger than the scan

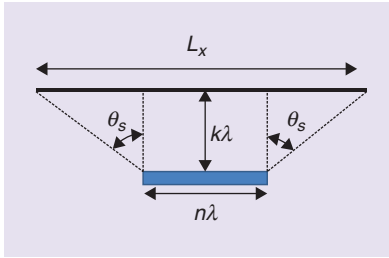


FIGURE 13. The geometry of a PNF.

plane. As typical, 2λ is the separation to the absorber tips. The width of the range becomes

$$W = (n + 2k \tan(\theta_s) + 4 + 2t_s)\lambda + \Delta_{scn}, \quad (21)$$

which can be rewritten as

$$W = L_x + (4 + 2t_s)\lambda + \Delta_{scn}, \quad (22)$$

where Δ_{scn} is the additional space required for the scanner structure, and t_s is the thickness of the absorber.

The length of the range is given by

$$L = S_{clr} + A_d + (4 + k + t)\lambda, \quad (23)$$

where S_{clr} is the scanner depth, which should include the spacing to the

absorber (if any; the scanner can be placed very close to the tips), and the probe length. A_d is the depth of the AUT and the support structure for aligning that antenna with the scanner. The 4λ in (23) is the space between the back of the AUT and the range wall. For antennas with very high gain, this wall does not need absorber treatment. But if desired, the thickness of the absorber for this wall can be as small as $\lambda/4$. The thickness of the absorber on the wall behind the scanner takes advantage of the directivity of the probe used to scan the plane. Thus, t in (23) can have values such that $t \geq 2$.

The remaining value to be defined is the absorber on the side walls. This is dependent on the angle θ_s and the factor k . We can approximate the width as

$$W \approx (n + 2k \tan(\theta_s) + 4 + 2t_s)\lambda \quad (24)$$

using the approximation that

$$(n + 2k \tan(\theta_s) + 4 + 2t_s)\lambda > \Delta_{scn}. \quad (25)$$

It follows that the angle of incidence on the side walls is

$$\theta = \arctan\left(\frac{k}{kn + k \tan(\theta_s) + 4}\right). \quad (26)$$

Notice that the angle of incidence is only dependent on the size of the AUT, the maximum angle for accurate far field, and the test distance in wavelengths. Figure 14 shows that even at ten wavelengths for a test distance, the largest angle of incidence is close to 20° . Figure 4 shows that the reflectivity of a given piece of absorber of a certain electrical thickness does not deteriorate much within that range of angles of incidence. If the AUT is a simple passive antenna, the high gain can be beneficial. Since the antenna will not radiate much energy to the side walls, a smaller absorber with $t < 1$ may be used. However, if the AUT is a complex antenna with beam steering, then the side walls should have a thickness such that $t \geq 2$.

In some cases, the scan distance is different in a vertical or horizontal orientation. Therefore, it is not rare for the chamber to not have a square cross section. The equation for the height becomes

$$H = L_y + y_o + (2 + t_s)\lambda, \quad (27)$$

where y_o is the minimum height of the probe, that is, the location of the probe at the bottom of the vertical motion. This includes the rails on which the scanner moves in the horizontal position and also should be large enough to include the floor absorber, so, at a minimum, $y_o > t_s$. CNF ranges will not be discussed in this article. The aforementioned rules for SNF and PNF ranges can be combined to arrive at a range size for a CNF system.

CONCLUSIONS

The goal of this article is to provide an overview of the rules and physics that guide the selection and sizing of indoor anechoic chambers. All of the equations provided in this article are approximations. The chamber length calculated using (9), (13), (16), (20), and (23) is a minimum, and more space may be required to help with the loading and unloading of the device-under

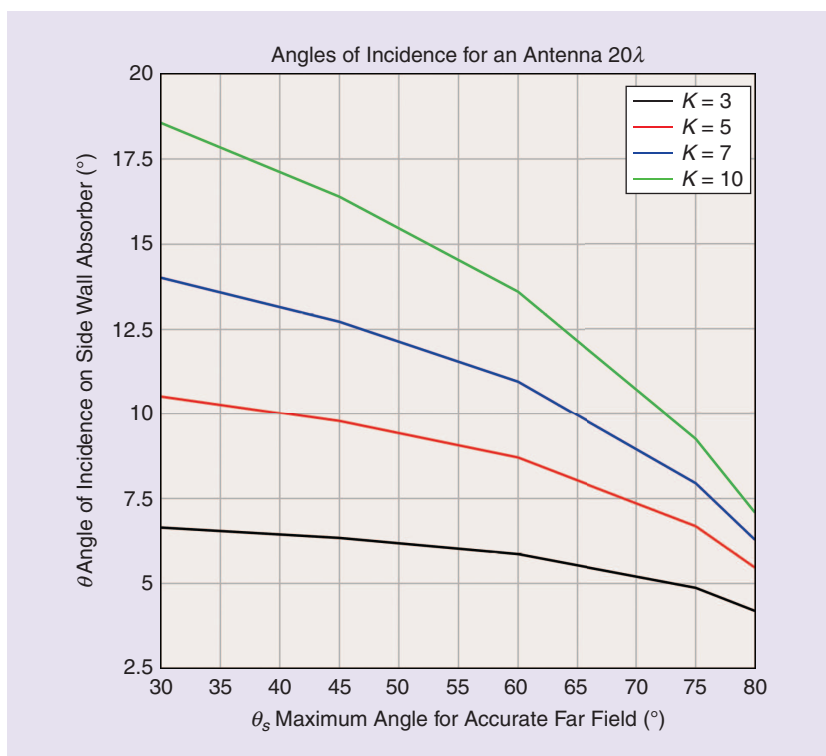


FIGURE 14. The angles of incidence on the absorber as a function of the maximum angle for accurate far-field pattern. Plotted for different test distances.

test, changing of feeds, range antennas, and connecting additional equipment. The polynomial equations have a margin of safety included in their results. This margin of safety helps in accounting for secondary bounces and edge diffractions as well as light fixtures, vents, doors, and other disruptions of the absorber treatment.

ACKNOWLEDGMENT

We would like to thank Zhong Chen for providing the computed results based on the algorithm introduced in [9].

AUTHOR INFORMATION

Vince Rodriguez (vrodiguez@nsi-mi.com) earned his B.S.E.E. degree in 1994 from the University of Mississippi, Oxford. He earned his M.S. and Ph.D. degrees in engineering science with an emphasis in electromagnetics in 1996 and 1999, respectively, from the University of Mississippi. In November 2014, he joined MI Technologies in Suwanee, Georgia, as a senior applications engineer. He is a Senior Member of the IEEE.

REFERENCES

- [1] L. Hemming, *Electromagnetic Anechoic Chambers: A Fundamental Design and Specification Guide*. Piscataway, NJ: IEEE Press, 2002.
- [2] G. Sanchez and P. Connor, "How much is a dB worth?" in *Proc. 23rd Annu. Symp. Antenna Measurement Techniques Association (AMTA 2001)*, Denver, CO, Oct. 2001, pp. 32–36.
- [3] J. Hansen and V. Rodriguez, "Evaluate antenna measurement methods," *Microwave RF*, pp. 62–67, Oct. 2010.
- [4] W. Stutzman and G. Thiele, *Antenna Theory and Design*, 2nd ed. New York: Wiley, 1997.
- [5] IEEE Standard Test Procedures for Antennas IEEE, ANSI/IEEE STD 149-1979 149-1979, 1979, reaffirmed 2008.
- [6] D. Wayne, J. Fordham, and J. McKenna, "Effects of non-ideal plane wave on compact range measurements," in *Proc. 36th Annu. Antenna Measurement Techniques Association Symp. AMTA 2014*, Tucson, AZ, Oct. 2014, pp. 63–68.
- [7] V. Rodriguez, G. d'Abreu, and K. Liu, "Measurements of the power handling of RF absorber materials: Creation of a medium power absorber by mechanical means," in *Proc. 31st Annu. Antenna Measurement Techniques Association Symp. AMTA 2009*, Salt Lake City, UT, Oct. 2009, pp. 220–224.
- [8] W. Sun and C. Balanis, "Analysis and design of periodic absorbers by finite-difference frequency-domain method," Telecommunications Research Center, Arizona State Univ., Tempe, AZ, Rep. TRC-EM-WS-9301, 1993.
- [9] E. Kuester and C. Holloway, "A low-frequency model for wedge or pyramid absorber arrays-I: Theory," *IEEE Trans. Electromagn. Compat.*, vol. 36, no. 4, pp. 300–306, Nov. 1994.
- [10] V. Rodriguez, "A study of the effect of placing microwave pyramidal absorber on top of ferrite tile absorber on the performance of the ferrite absorber," in *Proc. 19th Annu. Review Progress Computational Electromagnetics (ACES 2003) Symp.*, Monterey, CA, Mar. 2003, pp. 815–818.
- [11] W. Emerson and H. Sefton, "An improved design for indoor ranges," *Proc. IEEE*, vol. 53, no. 8, pp. 1079–1081, 1965.
- [12] H. King, F. Shiukuro, and J. Wong, "Characteristics of a tapered anechoic chamber," *IEEE Trans. Antennas Propag.*, vol. 15, no. 3, pp. 488–490, 1967.
- [13] V. Rodriguez, "Using tapered chambers to test antennas," *Evaluation Eng.*, vol. 43, no. 5, pp. 62–68, 2004.
- [14] J.-R. J. Gau, D. Burnside, and M. Gilreath, "Chebyshev multilevel absorber design concept," *IEEE Trans. Antennas Propagat.*, vol. 45, no. 8, pp. 1286–1293, 1997.
- [15] T.-H. Lee and W. Burnside, "Performance trade-off between serrated edge and blended rolled edge compact range reflectors," *IEEE Trans. Antennas Propag.*, vol. 44, no. 1, pp. 87–96, Jan. 1996.
- [16] D. W. Hess, "Near-field experience at Scientific-Atlanta" in *Proc. 1991 Symp. Antenna Measurement Techniques Association (AMTA 91)*, Boulder, CO, Oct. 1991, pp. 5–3–5–8.
- [17] A. Yaghjian, "An overview of near-field antenna measurements," *IEEE Trans. Antennas Propag.*, vol. AP-34, no. 1, pp. 30–45, Jan. 1986.
- [18] J. E. Hansen, Ed. *Spherical Near-Field Antenna Measurements*. London, United Kingdom: IEEE Peter Peregrinus, 1988.

Antenna Applications Corner

(continued from page 81)

Catania, Italy, since 2014. His research interests include the development of ultra-wideband compact antennas, microwave devices, and computational electromagnetism, with particular interest in radio-frequency plasma interactions and particle accelerators.

REFERENCES

- [1] H. Stockman, "Communication by means of reflected power," *Proc. Inst. Radio Engineers*, vol. 36, no. 10, pp. 1196–1204, 1948.
- [2] G. S. Mauro, G. Castorina, A. F. Morabito, L. Di Donato, and G. Sorbello, "Effects of lossy background and rebars on antennas embedded in concrete structures," *Microwave Opt. Technol. Lett.*, vol. 58, no. 11, Nov. 2016.
- [3] R. W. P. King, G. S. Smith, M. Owens, and T. T. Wu, *Antennas in Matter: Fundamentals, Theory, and Applications*. Cambridge, MA: MIT Press, 1981.
- [4] H.-Y. Liang, H.-C. Yang, and J. Zhang, "A cylindrical conformal directional monopole antenna for borehole radar application," *IEEE Antennas Wireless Propag. Lett.*, vol. 11, pp. 1525–1528, Dec. 2012.
- [5] C. Liu, Y. Guo, and S. Xiao, "Capacitively loaded circularly polarized implantable patch antenna for ISM-band biomedical applications," *IEEE Trans. Antennas Propag.*, vol. 59, no. 1, pp. 177–199, Jan. 2011.
- [6] D. Pinchera, M. D. Migliore, and F. Schettino, "An ultra wide permittivity antenna (UWPA) for reliable through-wall communications," *IEEE Trans. Antennas Propag.*, vol. 61, no. 2, pp. 957–960, Oct. 2012.
- [7] M. Rad and L. Shafai, "Embedded microstrip patch antenna for structural health monitoring applications," presented at the IEEE Antennas and Propagation Society Int. Symp., San Diego, CA, July 2008.
- [8] X. Jin and M. Ali, "Reflection and transmission properties of embedded dipoles and PIFAs inside concrete at 915 MHz," presented at the IEEE Antennas and Propagation Society Int. Symp., Charleston, SC, June 2008.
- [9] S.-H. Jeong and H.-W. Son, "UHF RFID tag antenna for embedded use in a concrete floor," *IEEE Antennas Wireless Propag. Lett.*, vol. 10, pp. 1158–1161, Oct. 2011.
- [10] S. Jiang and S. V. Georgakopoulos, "Optimum wireless power transmission through reinforced concrete structure," in *Proc. IEEE Int. Conf. Radio-Frequency Identification*, Orlando, FL, 2011, pp. 11–18.
- [11] F. Abboud, J. Damiano, and A. Papernik, "Simple model for the input impedance of coax-fed rectangular microstrip patch antenna for CAD," *IEE Proc. H Microwaves Antennas Propagat.*, vol. 135, no. 5, pp. 323–326, Nov. 1988.
- [12] L. Kosuru and D. Deavours, "Optimum performance for RFID tag immersed in dielectric media," in *Proc. IEEE Int. Conf. Radio-Frequency Identification*, Orlando, FL, 2011, pp. 11–18.
- [13] M. Deshpande and M. Bailey, "Input impedance of microstrip antennas," *IEEE Trans. Antennas Propag.*, vol. 30, no. 4, pp. 645–650, July 1982.
- [14] C. A. Balanis, *Antenna Theory: Analysis and Design*. Hoboken, NJ: Wiley, 2012.
- [15] R. Garg and S. Long, "Resonant frequency of electrically thick rectangular microstrip antennas," *Electron. Lett.*, vol. 23, no. 21, pp. 1149–1151, July 1987.
- [16] R. Sorrentino and G. Bianchi, *Microwave and RF Engineering*. Hoboken, NJ: Wiley, 2010.
- [17] F. Abboud, J. Damiano, and A. Papernik, "Simple model for the input impedance of coax-fed rectangular microstrip patch antenna for CAD," *IEE Proc. H Microwaves Antennas Propagat.*, vol. 135, no. 5, pp. 323–326, Nov. 1988.
- [18] I. Wolff and N. Knoppik, "Rectangular and circular microstrip disk capacitors and resonators," *IEEE Trans. Microw. Theory Techn.*, vol. 22, no. 10, pp. 857–864, Oct. 1974.
- [19] J. J. Wang, Y. P. Zhang, K. M. Chua, and A. C. W. Lu, "Circuit model of microstrip patch antenna on ceramic land grid array package for antenna-chip codesign of highly integrated RF transceivers," *IEEE Trans. Antennas Propag.*, vol. 53, no. 12, pp. 3877–3883, Dec. 2005.